The Astronomical Journal, 138:1435–1441, 2009 November doi:10.1088/0004-6256/138/5/1435

MASS TRANSFER VARIATIONS IN UX MONOCEROTIS: EIGHT YEARS OF AUTOMATED PHOTOMETRIC MONITORING

EDWARD C. OLSON[1], GREGORY W. HENRY[2], AND PAUL B. ETZEL[3]
[1] Astronomy Department, University of Illinois, 1002 W. Green St., Urbana, Illinois 61801-3074, USA; olsomed@astro.illinois.edu
[2] Tennessee State University, Center of Excellence in Information Systems, 3500 John A. Merritt Blvd., Box 9501, Nashville, TN 37209, USA; henry@schwab.tsuniv.edu
[3] Astronomy Department, San Diego State University, San Diego, California 92182, USA; etzel@sciences.sdsu.edu
Received 2009 January 27; accepted 2009 August 13; published 2009 October 2

ABSTRACT

We analyze eight years (1999–2007) of automated photometric observations of the active Algol binary UX Monocerotis to search for mass transfer bursts similar to those seen in U Cephei. The largest photometric anomaly is the mean gainer luminosity difference between the stream-impact hemisphere and the opposite hemisphere. We find an updated Wilson–Devinney solution for earlier six-color observations. The UX Mon donor star fills its Roche lobe and the gainer nearly fills its rotational lobe. Instead of isolated bursts of the U Cep type, we found nearly continuous brightness fluctuations likely produced by variable mass transfer. We discuss implications for mass transfer.

Key words: binaries: eclipsing – stars: individual (UX Monocerotis) – techniques: photometric

Online-only material: machine-readable and VO tables

1. INTRODUCTION

The Algol eclipsing binary U Cephei (HD 5679; $P = 2.49$ day; B7V+G8III-IV) undergoes occasional mass transfer bursts producing large, optically thick, disturbances in its photosphere (Olson 1985). During a burst, the mass-transferring stream strikes the more massive gainer star and penetrates below its photosphere. Accretion energy deposited there raises the radiation pressure and produces a prominent equatorial bulge whose light distorts the shape of the normally total primary eclipse. Its mass ratio, q (donor/gainer), is about 0.6, larger than that of many Algols.

Olson & Etzel (1995) discussed *Iybvu* photometry of the totally eclipsing binary UX Monocerotis (HD 65607; $P = 5.90$ day; A5III-IVe+G2III) that showed it to be an Algol with a photometric mass ratio of about 0.8. The mass-transferring stream strikes the gainer but at a more nearly grazing angle. We update our solution to the earlier data.

We suspected that even stronger transfer bursts might occur in UX Mon than in U Cep, given the larger mass ratio of the former. Therefore, we obtained eight years of automated photometric telescope (APT) V and B observations beginning in 1999 September. The APT light curves display considerable photometric activity, most obvious outside primary eclipse but also extending, with reduced amplitude, into eclipse. We discuss the temporal and phase behavior of these variations and suggest variable mass transfer as a plausible explanation. We discuss smaller brightness variations of the cool donor star (star 2), visible in primary eclipse totality, and summarize implications for mass transfer.

2. A NEW SIX-COLOR PHOTOMETRIC SOLUTION

A number of improvements prompted us to refine our earlier Wilson–Devinney (WD) (Wilson 1992) solution for UX Mon (Olson & Etzel 1995). Faster computers make finer integration grids (≈63,63,63,63) practical while retaining the symmetrical-derivative option (WD control integer ISYM = 1). We introduced improved theoretical stellar fluxes by convoluting our intermediate filter passbands, atmospheric transmission, photomultiplier response, aluminum reflectivity, and model atmosphere fluxes (R. L. Kurucz 1996, private communication) into the WD code. We also used (linear) limb-darkening coefficients (Van Hamme 1993) derived from the same atmosphere grid. Our v filter is centered near 4200 Å to avoid the stellar Hδ line. The I filter has central wavelength 8425 Å and total halfmax width 500 Å. We therefore used instrumental (natural) magnitudes, corrected for differential extinction, in all WD solutions. These modifications yielded a more accurate mean donor temperature, T_2.

We omitted the ultraviolet observations, which contain circumstellar Balmer continuum emission, from our solutions. We added less complete observations made with Etzel's intermediate-band filters in the red and near infrared (r, 6870 Å; and i, 7950 Å).

The ephemeris remains unchanged. Because of changing light-curve distortions, we obtained a single mean time of mid-primary eclipse using all of our eclipse data:

HJD(pri) = 2 448 001.6126 ±0.0008.

WD phase-shift parameter, PSHIFT, gave a phase correction of 0.0001, corresponding in time to about 0.9 min.

As the APT observations show, UX Mon undergoes appreciable brightness fluctuations on time scales of weeks to months. For a reliable WD solution, the data must be binned in phase to average over these variations. We selected bins of width 0.002 in primary eclipse, 0.01 in secondary eclipse, and 0.02 outside eclipses, yielding a maximum of 150 bins. Individual *Iybvri* observations are listed in Table 1.

At the time of our earlier observations, 1988 January to 1992 February, light levels between phases ≈0.4 and 1.2 were appreciably brighter than those around phase 0.3, as shown in Figure 2 of Olson & Etzel (1995). The same plot shows observations of Hiltner et al. (1950) made some 40 years earlier. The latter light curve looks nearly normal with respect to light levels at quadrature. Donor light was essentially unchanged in this interval, so gainer light, centered on the stream-impact hemisphere, had brightened.

Contact points in semidetached, totally eclipsing binaries strongly constrain binary parameters. We verified this point by doing solutions that included a variety of data points outside

Table 1
Iybvuri Observations of UX Monocerotis

HJD (2400000+)	Δ (mag)	HJD (2400000+)	Δ (mag)	HJD (2400000+)	Δ (mag)	HJD (2400000+)	Δ (mag)
47181.71725	−0.007	47186.72414	0.606	47186.87454	0.602	47204.72371	0.449
47181.71825	−0.006	47186.72746	0.619	47186.87717	0.588	47204.72675	0.451
47181.72240	−0.012	47186.72840	0.603	47186.88083	0.583	47204.72763	0.447
47181.72350	−0.004	47186.73197	0.632	47186.88361	0.597	47204.73121	0.441
47181.73911	−0.045	47186.73286	0.599	47186.88727	0.587	47204.73220	0.430

Notes. Observations in a given filter are grouped together; a header for each page lists the filter.

(This table is available in its entirety in machine-readable and Virtual Observatory (VO) forms in the online journal. A portion is shown here for guidance regarding its form and content.)

Table 2
Wavelength-independent Parameters, UX Mon[a]

Parameter	Value	Parameter	Value	Parameter	Value	Parameter	Value	Parameter	Value
T_1	8000K	g_1	1.00	F_1	5.5	r_1(pl)	0.170	r_2(pl)	0.336
T_2	5500K	g_2	0.32	F_2	1.0	r_1(pt)	0.223	r_2(pt)	0.475
Ω_1	6.663	A_1	1.00	i	84.7	r_1(sd)	0.215	r_2(sd)	0.352
Ω_2	3.391	A_2	0.40	q	0.785	r_1(bk)	0.221	r_2(bk)	0.384

Note. [a] *Iybvri* solutions; PSHIFT = 0.0001.

primary eclipse. Except for gainer luminosity, L_1, parameters (including mass ratio) usually agreed to within their estimated mean errors. Since primary eclipse falls in the "bright" range of outside-eclipse observations, we included only these data (that is, in phase range 0.4–1.2) in WD solutions.

The sum of the weighted squared light residuals, SR, remains the solution criterion. Other observational details are in Olson & Etzel (1995).

We assumed a semidetached configuration with the less massive donor star (star 2) filling its Roche lobe (WD MODE 5) and later checked this assumption. In most iterations, we decoupled T_2 from donor luminosities L_2 (IPB = 1) (making them variable parameters), because even modern atmosphere fluxes may not match observations at, or below, the 1% level. Close to solution convergence we coupled these parameters to update T_2.

Main MODE 5 system parameters are F_1 (actual/synchronous gainer equatorial rotation), i (inclination), Ω_1 (gainer potential), q (mass ratio, donor/gainer), L_1, and L_2. We assume $F_2 = 1.0$. Large parameter correlations may hamper solution convergence (Wilson 1992), even using a damped least-squares routine (Kallrath et al. 1998). We explored a number of parameter subsets. Those including F_1 and q gave correlation coefficients between Ω_1 and q of about 0.98, so we fixed F_1 at a series of values. At each F_1 we obtained solutions over a range of assumed q, selecting the one with the smallest SR. The F_1 solution with smallest SR then became the best solution. We also adjusted gravity exponent g_2, bolometric albedo A_2, and limb-darkening coefficients x_1 and x_2. Results are listed in Tables 2–5.

We checked the donor lobe-filling condition by doing solutions with assigned Ω_2 slightly larger than the lobe-filling value (thereby detaching the donor from its lobe). Results are consistent with lobe filling; solution SR were the same from $\Omega_2 = 3.391$ (lobe filling) to 3.40, and then increased with increasing Ω_2.

With respect to potentials, the gainer fills 98% of its rotational lobe. Mean errors were found from an iteration with all main parameters, including F_1 and q. The T_2 mean error (10 K) was found from WD solutions with individual filters, in which other parameters were fixed at their values from the six-color

Table 3
Wavelength-dependent Parameters, UX Mon[a]

Parameter	I	y	b	v	r	i
x_1	0.23	0.46	0.55	0.60	0.31	0.21
x_2	0.47	0.61	0.75	1.03	0.36	0.32
L_1[b]	5.76	8.55	10.08	11.71	6.96	6.16
L_2[b]	7.47	5.60	4.65	3.41	6.82	7.40
l_{1q}[c]	0.385	0.535	0.611	0.704	0.447	0.403
l_{2q}[c]	0.615	0.465	0.389	0.296	0.553	0.597

Notes.
[a] *Iybvri* solution; $l_3 = 0.000$.
[b] 4π luminosities.
[c] Fractional lights at quadrature.

Table 4
Fundamental Parameters

Parameter	Star 1	Star 2
$M/M_\odot$	2.51	1.97
$R/R_\odot$	4.47	8.12
M_{bol}	0.1	0.4
log g(cgs)	3.5	2.9
v_{syn}[a]	38.0	69.0
$v \sin i$	209.0	69.0

Note. [a] km s^{-1}; mean radii.

solution. The average of these T_2 agreed well with the adopted one found from the simultaneous solution. Weighted mean magnitude deviations from solution light curves ranged from ±0.016 mag to ±0.035 mag. These errors are about twice those of less-disturbed Algols and imply lower solution reliability.

Within the estimated mean error spreads, main system parameters almost overlap those of Olson & Etzel (1995), except for the inclination (in the earlier solution, there may have been a problem with correlation coefficients or with iterations with L_2 coupled to T_2 through an older atmosphere grid).

Figure 1 shows y observations (normal points) and the WD y solution (full curve). The derived mass ratio is set mainly by primary eclipse contact points and not by the out-of-eclipse curvature, though it is encouraging that this curvature is well

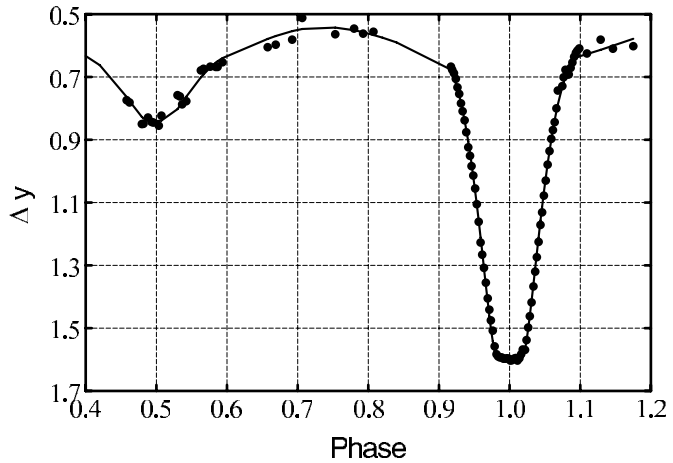

Figure 1. Intermediate-band *y* observations (normal points) from Olson & Etzel (1995) and updated WD solution (full curve) for UX Mon. Phases used are in the bright region associated with stream impact (see text).

Table 5
Parameter Mean Errors, UX Mon

Parameter	Error
F_1(phot)	0.3
i	0.3
T_2[a]	10.0
Ω_1	0.1
$L_1(I)$	0.12
$L_1(y)$	0.27
$L_1(b)$	0.37
$L_1(v)$	0.49
$L_2(I)$	0.03
$L_2(y)$	0.02
$L_2(b)$	0.02
$L_2(v)$	0.02
$M/M_\odot(1)$	0.16
$M/M_\odot(2)$	0.14
$R/R_\odot(1)$	0.12
$R/R_\odot(2)$	0.19

Note. [a] K.

fit by the solution. Out-of-eclipse scatter derives from the photometric variations already mentioned.

3. APT OBSERVATIONS

We acquired new photometry of UX Mon with the T3 0.4 m APT at Fairborn Observatory in southern Arizona. The precision photometer for the T3 APT is based around a temperature-stabilized EMI 9924B bi-alkali photomultiplier tube detector, which counts photons through Johnson *B* and *V* filters. The APT is programmed to measure stars in the following sequence, termed a group observation: *K, sky, C, V, C, V, C, V, C, sky, K*, where *K* is a check star, *C* is the comparison star, and *V* is the program star. More than 800 group observations of UX Mon were obtained with the APT during eight observing seasons between 1999 September and 2007 May. HD 65199 ($V = 7.67$, $B - V = -0.08$) served as the comparison star and HD 65938 ($V = 6.45$, $B - V = 0.84$) as the check star.

To create group means for each group observation, three variable minus comparison ($V - C$) and two check minus comparison ($K - C$) differential magnitudes in each photometric band were computed and averaged. The group means were then corrected for differential extinction with nightly extinction coefficients, transformed to the Johnson system with yearly mean transformation coefficients, and treated as single observations thereafter. The external precision of the group means, based on standard deviations for pairs of constant stars, is typically ~0.004 mag on good nights with this telescope. Group mean differential *B* and *V* magnitudes with internal standard deviations greater than 0.01 mag were discarded, leaving 749 and 704 good group means in *B* and *V*, respectively. These individual differential magnitudes are listed in Table 6. Further details of our automatic telescope operations and data-reduction procedures can be found in Henry (1995a), Henry (1995b), and Eaton et al. (2003).

Comparison *B* and *V* counts for 10-second integrations, which were about 530,000 and 300,000, respectively, so photon statistics adds only about 0.003 mag to errors in primary eclipse totality.

Table 6
APT Photometric Observations of UX Mon

Hel. Julian Date (HJD − 2,400,000) (1)	$(V-C)_B$ (mag) (2)	$(V-C)_V$ (mag) (3)	$(K-C)_B$ (mag) (4)	$(K-C)_V$ (mag) (5)
51473.9830	1.229	0.772	−0.318	−1.217
51474.9318	1.215	0.724	−0.320	−1.215
51475.9478	1.219	0.786	−0.320	−1.217
51476.9246	1.360	99.999	99.999	99.999
51477.9403	1.158	0.671	−0.319	−1.211

Notes. A "99.999" in any column signifies that the standard deviation of that observation exceeds 0.01 mag and is not used.

(This table is available in its entirety in machine-readable and Virtual Observatory (VO) forms in the online journal. A portion is shown here for guidance regarding its form and content.)

4. DISCUSSION OF APT OBSERVATIONS

The APT observations display a variety of time- and phase-dependent brightness variations. Brightness variations are somewhat larger in *B* than in *V*. The coverage of primary eclipse was sparse and spread over eight seasons. Brightness variations (scatter) and observational undersampling yielded an asymmetrical eclipse curve. The ephemeris of Olson & Etzel (1995) placed the upper, brighter, half of eclipse near phase 0.0. We reduced the epoch by 0.028 day to center graphically the fainter half of eclipse (less affected by gainer brightness fluctuations) at phase 0.0. We then derived an approximate mean time of minimum in Heliocentric Julian days (and a large eclipse-asymmetry error):

HJD(pri) = 2 452 825.539 ±0.012.

It is premature to interpret mass transfer-related period changes in UX Mon.

Figure 2 shows all APT *B* observations of UX Mon. As noted above, group mean differential magnitudes with internal standard deviations greater than 0.01 mag were discarded, so observational errors are small compared with the scatter in Figure 2. The check-comparison magnitudes statistics are: *V*, $N = 617$, $\sigma = 0.0060$ and for *B*, $N = 668$, $\sigma = 0.0058$. A separate plot of check-comparison magnitudes, at the same scale as in Figure 1, confirms this point.

V data yield a similar plot, with slightly smaller variations.

Primary eclipse asymmetry is apparent in Figure 2 (and absent in Figure 1). Photometric scatter, largest outside primary eclipse, contains time changes on a scale of weeks to years. Light near mid-primary eclipse is more nearly constant. (An approximate WD solution reveals short-term variations persisting in primary

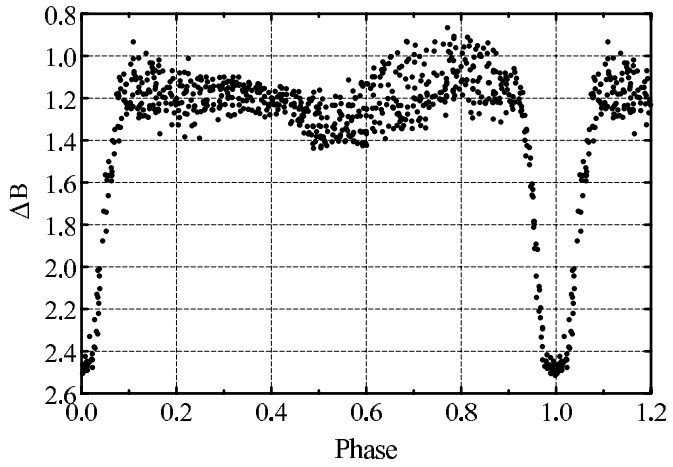

Figure 2. All individual APT *B* observations of UX Mon.

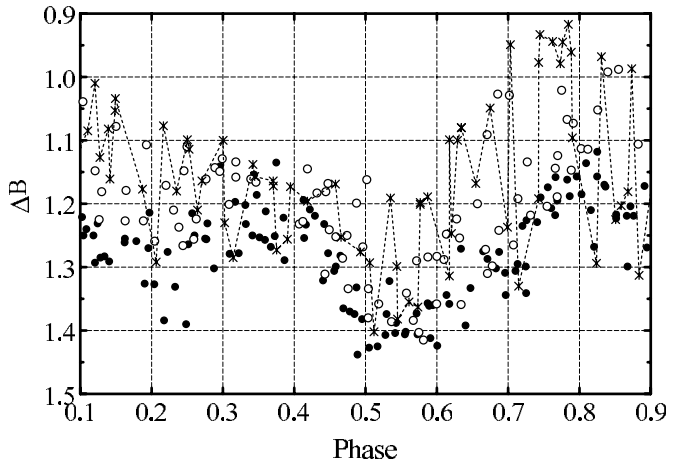

Figure 3. APT *B* observations outside primary eclipse: season 1 (1999–2000, filled circles); season 4 (2002–2003, open circles); season 8 (2006–2007, asterisks connected by dashed lines).

eclipse and decreasing in size toward totality, in spite of the casual impression given by Figure 2.) This behavior is consistent with the comments of Hiltner et al. (1950). Since they affect broad-band *B* and *V* light, brightness variations are optically thick in the continuum and probably originate in or near the gainer photosphere.

Photometric scatter is largest near phases 0.7–0.8, when the gainer's stream-impact hemisphere is most directly visible. Scatter is smallest near phases 0.3–0.45, when the stream-impact hemisphere is largely hidden. The hemispheric origin of light at any phase limits spatial resolution in gainer longitude; time resolution is set by observing conditions. Later, we restrict our discussion to the above two hemispheres, which we label "stream-impact" and "stream-hidden."

Points in any phase range in Figure 2 may include observations made at times scattered through all eight observing seasons. Separating observations by season is the first step toward a clearer picture of temporal changes.

Figure 3 shows *B* light curves outside primary eclipse for seasons 1 (filled circles), 4 (open circles), and 8 (asterisks connected by dashed lines). Adding observing seasons increases plot congestion without adding much relevant detail.

Photometric scatter increases from seasons 1 to 8 and is largest near phases 0.7–0.8. At the scale of Figure 3, brightness maxima resemble "sharp peaks" when points are connected, as in season 8.

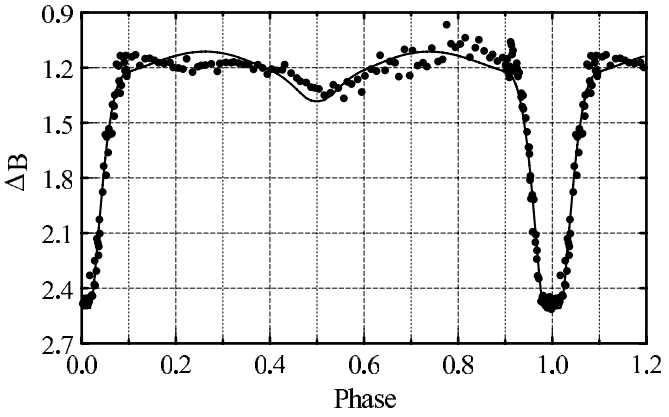

Figure 4. APT *B* observations and WD solution (solid curve; see text).

By chance season 1, with the smallest photometric scatter, has the largest number of *B* observations (148). These data roughly define a "lower scatter envelope" in Figure 3. The shape of this envelope resembles light variations outside primary eclipse predicted by the WD photometric solution (observed amplitude is somewhat larger). The faintest points from seasons 4 and 8 also tend to mix with this lower envelope, allowing for intrinsic scatter, finite time resolution, and the modest number of points per season (111 in season 4; 80 in season 8). Scatter in this lower envelope is at least ±0.05 mag. Phase range 0.1–0.25 remains questionable because of outliers.

A corresponding plot for *V* observations generally confirms these arguments (secondary eclipse is deeper and the amplitude of sharp peaks is smaller).

Brightness changes with orbital phase may therefore consist of a slow variation of the lower envelope, upon which sharp brightness peaks are superimposed. A mean light curve obtained in season 8 would brighten by the average of many sharp peaks, the largest increase being near phases 0.7–0.8, where peak heights reach nearly 0.3 mag (or possibly more with finer time resolution). An effective luminosity difference would exist between gainer hemispheres. Most observations were made under such conditions.

Olson & Etzel (1995) also noted that the ultraviolet brightness maximum near phase 0.7 was more pronounced than at longer wavelengths, suggesting heating by stream impact. This maximum was absent in a few observations, as though impact heating had temporarily ceased. These variations were about 0.3 mag, so data are consistent with variable impact heating. It is plausible to associate brightness maxima, which are largest in the stream-impact hemisphere, with mass transfer bursts, as we initially assumed.

A WD light curve solution for APT observations illustrates these effects. We averaged observations into bins of phase width 0.001 in primary eclipse and 0.01 outside eclipse, giving 183 *B* normal points (most normal points in primary eclipse contain only one or two observations). Including observations at all phases (unlike the *y* results in Figure 1) averages L_1 over all gainer longitudes. We obtained a simultaneous *VB* solution by fixing gainer F_1, *i*, and *q* at values given by our updated solution, and varying L_1 and L_2. Figure 4 shows *B* normal points and solution (full curve). The nature of the sharp brightness peaks shown in Figure 3 partly accounts for the deviations from the calculated light curve in Figure 4. The mean hemispheric luminosity near phase 0.25 is smaller than that near 0.75.

This solution procedure is justified. As already noted, for a totally eclipsing binary, eclipse contacts strongly constrain the

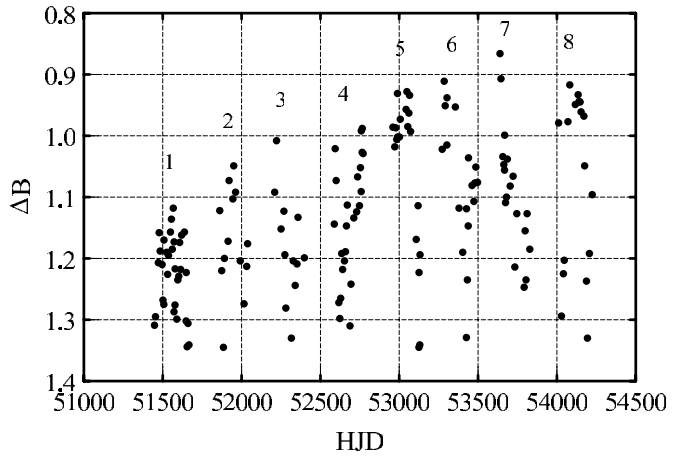

Figure 5. Time variations from APT *B* observations in the orbital phase range 0.657–0.859. Observing seasons are labeled.

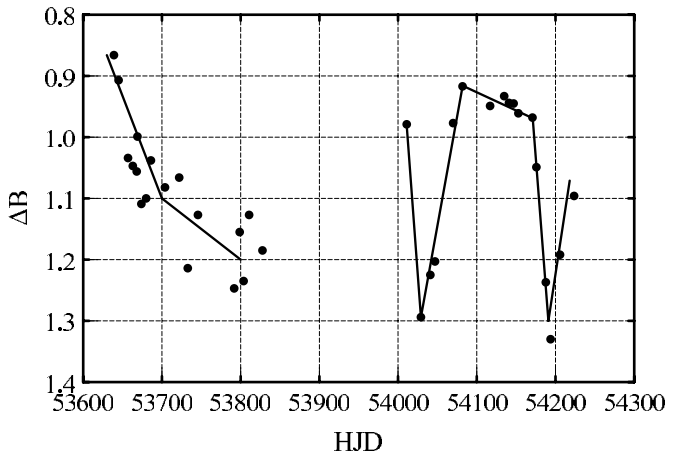

Figure 6. APT *B* observations in seasons 7 and 8 of the campaign. Line segments represent variations within the estimated errors.

solution. Donor lobe-filling fixes the photometric mass ratio, which is only slightly affected by "ellipsoidal" variation outside eclipses.

In Figure 3, single-season observations in a fixed phase range were made at a mix of times during the season. For such a phase range, plotting ΔB versus HJD shows time variations explicitly. The phase range must be large enough to contain a reasonable number of observations, but small enough to restrict observations to a modest spread in gainer longitude. We used a phase range of about 0.2. Resulting light curves are slightly perturbed by the phase-dependent brightness change in the lower envelope scatter. A single ΔB therefore has an estimated error $\leqslant \approx 0.05$ mag.

As noted above, we selected two phase ranges (in all seasons) to cover regions of maximum and minimum scatter: phases 0.657 to 0.859 ("stream impact"), 154 observations; and 0.230 to 0.452 ("stream hidden"), 155 observations.

Figure 5 shows *B* observations from the stream-impact region. Observing seasons are numbered on the plot; plotted HJD are actual HJD-2 400 000. Most variations are appreciably larger than the estimated error. The upper scatter envelope (not to be confused with scatter envelopes in Figure 3) brightened from seasons 1 to 7 by about 0.25 mag, while in season 8 maximum brightness declined slightly. The lower envelope brightness was essentially constant, but the number of those observations

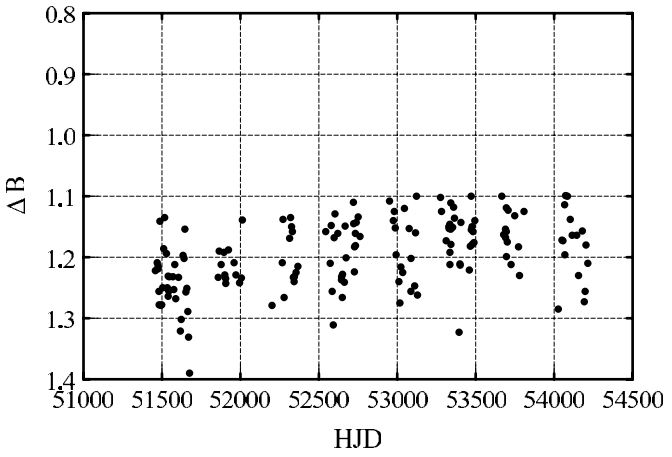

Figure 7. Time variations from APT *B* observations in the phase range 0.230–0.452. Scale is the same as that in Figure 5.

is small. Maximum brightness variations are about 0.4 mag, though finer time resolution might have increased this range.

The timescale of Figure 5 must be expanded to show variations clearly. The "error" in HJD is effectively zero, so we map brightness variations constrained by the estimated error in ΔB. Data from seasons 7 (left group) and 8 are plotted on an expanded HJD axis in Figure 6. Given the above error estimate, we fit most variations with the straight-line segments in Figure 6. A few points lie more than 0.05 mag from line segments (assuming a smaller error could lead to more line segments and increased variability). In season 8, brightness changes of order ± 0.2 to ± 0.4 mag occurred on time scales of a few tens of days, though seasonal gaps prevented complete coverage. Only in season 7 did the brightness appear to decline steadily. Plots of *V* data in the same phase ranges mirror *B* plots fairly well.

Light curves may contain monotonic brightness "drops" and "rises" larger than 0.1 mag, and "quiescent" periods with brightness changes less than 0.1 mag, as shown in Figure 6 for season 8. Changes in season 1 are small. For seasons 2–8, we find a total of 10 drops of duration 58 ± 47(sd) days and size $+0.29 \pm 0.08$ mag; seven rises of duration 46 ± 20 days and size -0.26 ± 0.08 mag; and four quiescent periods of duration 84 ± 23 days. Drops, rises, and quiescent periods fill 47%, 26%, and 27%, respectively, of the total observing time. The activity associated with growing and declining mass transfer bursts is therefore present some 73% of the time. These numbers are uncertain because the observational record is not continuous.

Figure 7 shows *B* brightness variations in the ("stream-hidden") phase range (0.230–0.452) for all eight seasons, scaled as in Figure 5. The lower envelopes are roughly the same (there are a few outliers near HJD 51520), and no ΔB is brighter than about 1.1, as though observations in the brighter half of Figure 5 had been removed.

Can brightness variations in the stream-hidden hemisphere be explained by mass transfer variations alone? In the stream-impact region, accretion energy from the low-density fringes of the mass-transferring stream dissipates in or near the photosphere. If the central-stream ram pressure were large enough (Lubow & Shu 1976), then matter also penetrates below the photosphere, degrades to produce a photon excess that is carried in gainer longitude (probably helped by supersynchronous gainer rotation), and gradually escapes as photons random walk to the surface. If the subsurface photon excess lasts a few days,

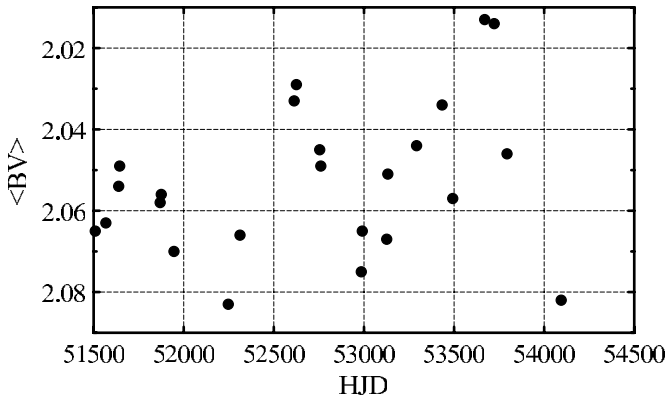

Figure 8. Means of APT *B* and *V* observations of the cool donor star in primary eclipse totality.

then excess radiation will be seen from the stream-hidden hemisphere. The impacting stream penetrates to a depth where ram pressure roughly equals the interior pressure (Ulrich & Burger 1976). The photon excess random walks to the surface in a diffusion time given by Shu (1982).

We calculated approximate diffusion times for radial steps through the outer parts of an interior model (similar to the UX Mon gainer) calculated by Dr. M. S. Hjellming and supplied by Dr. Ron Webbink. The photon diffusion time to the surface from fractional radial depth 0.08 is a few days. A peak transfer rate of about 10^{-5} solar masses per year is required. Such a peak rate may be possible, though improbable, for UX Mon.

Durations of transfer events are longer than a few days, so in a naive interpretation, light curves from stream-impact and stream-hidden hemispheres should show similar drops and rises. Stream-hidden light curves are uncertain because of their small variations. Only in seasons 7 and 8 could we identify matches over about half of each light curve. Matching fractions fell to about 0.2 for the remaining seasons. The likely turbulent nature of energy dissipation and reradiation may complicate the comparison. Inadequate time resolution of our observations adds uncertainty. We could therefore reach no firm conclusion about this crude picture. More realistic modeling is beyond the scope of this paper.

The early-G III-IV donor star in UX Mon is visible alone in primary eclipse totality, when 24 APT observations were made. Olson & Etzel (1993) observed brightness fluctuations in the cool donors of six totally eclipsing Algol binaries (period 1.0–9.5 days) over intervals of 7–14 years, suggesting the presence of rotationally induced magnetic activity. Recently, D. E. Mkrtichian et al. (2009, in preparation) discussed changes in the RZ Casssiopeia gainer (asteroseismic) oscillation spectrum, triggered by a mass transfer/accretion burst initiated by magnetic activity on its K0 donor ($P = 1.2$ day).

Figure 8 shows means of *B* and *V* observations in totality. We estimate an error (including photon statistical noise) of about 0.015 mag. There is no obvious phase dependence in these data; the two brightest points near HJD 53700 are at phases 0.9882 and 0.0078. The luminosity of the outer hemisphere of the donor star did seem to change appreciably during APT observations.

The mean durations of drops and rises in Figure 8 are longer than those noted above for gainer variations, so no direct correlation exists between donor and gainer brightness variations. Nevertheless, both Roche lobe overflow and magnetic activity may contribute to mass transfer and to the variety of brightness changes seen in the UX Mon gainer.

5. CONCLUSIONS

UX Mon brightness variations differ from those of U Cep during its transfer bursts. As noted, U Cep brightenings occur in primary eclipse, arising from prominent equatorial bulges that develop on the gainer. The main feature outside eclipse is a large drop in brightness, near phase 0.6, that deepens toward short wavelength. This feature may follow from bulge radiation normal to the orbital plane (not in the observer's line of sight), and cooling associated with the increased radiating area. We found similar, but smaller, bursts in the stream-impact Algol RW Tauri ($P = 2.77$ day) (Olson 1982), and hints of disturbances in several other short-period Algols. Among long-period Algols ($P >$ about 10 day), E. C. Olson & Etzel (2009, in preparation) conclude, from the behavior of Hα accretion disk emission, that small transfer bursts occur in these binaries as well.

In UX Mon, brightness variations are present in primary eclipse ingress and egress, but larger changes occur outside eclipse. UX Mon appears to be in a state of nearly continuous variable mass transfer, and its light curves are significantly more disturbed than those of U Cep between transfer bursts.

The geometry of stream impact in UX Mon may preclude formation of bulges of the U Cep type. Alternatively, the *mean* transfer rates of both binaries may be comparable. Mechanisms (associated with donor stars) that modulate mass flows may spread those of UX Mon more nearly uniformly in time. In U Cep, mass flows are less frequent, of shorter duration, and therefore may be sufficiently energetic to raise equatorial bulges on the gainer.

The large range of timescales, from days to entire observing seasons, exposes details in mass transfer and accretion processes in UX Mon. More frequent photometric observations, from different terrestrial longitudes and over entire observing seasons, would yield more nearly continuous coverage to reveal details that could contribute to a fuller understanding of these partly chaotic processes. Ultraviolet observations could be particularly helpful.

We thank the National Science Foundation for support through grants AST-8822351 and 9115033 (to E.C.O.) and AST-8822790, AST-9115104, and AST-9417035 (to P.B.E.). Partial support was provided by the University of Illinois and San Diego State University. G.W.H. acknowledges support from NASA, NSF, Tennessee State University, and the State of Tennessee through its Centers of Excellence program. Drs. Burt Nelson and Ron Angione, previous Directors of MLO, provided flexible observing time. The support staff efficiently maintained telescope and auxiliary equipment. NSF partially funded the CCD spectroscopic detection system. Dr. Bob Wilson supplied his eclipsing binary program and Dr. Bob Kurucz furnished fluxes from his model atmosphere grid. E.C.O. thanks Dr. Ron Webbink for access to interior models and the Department of Astronomy at the University of Illinois at Urbana-Champaign for an office in his emeritus years. We thank the referee for helpful comments on an early, shorter version of this paper.

REFERENCES

Eaton, J. A., Henry, G. W., & Fekel, F. C. 2003, in The Future of Small Telescopes in the New Millennium II. The Telescopes We Use, ed. T. Oswalt (Dordrecht: Kluwer), 189

Henry, G. W. 1995a, in ASP Conf. Ser. 79, Robotic Telescopes: Current Capabilities, Present Developments, and Future Prospects for Automated Astronomy, ed. G. W. Henry & J. A. Eaton (San Francisco, CA: ASP), 37
Henry, G. W. 1995b, in ASP Conf. Ser. 79, Robotic Telescopes: Current Capabilities, Present Developments, and Future Prospects for Automated Astronomy, ed. G. W. Henry & J. A. Eaton (San Francisco, CA: ASP), 44
Hiltner, W. A., Struve, O., & Jose, P. D. 1950, ApJ, 112, 504
Kallrath, J., Milone, E. F., Terrell, D., & Young, A. T. 1998, ApJ, 508, 308
Lubow, S. H., & Shu, F. H. 1976, ApJ, 207, L53
Olson, E. C. 1982, ApJ, 259, 702
Olson, E. C. 1985, in Interacting Binaries, ed. P. P. Eggleton & J. E. Pringle (Dordrecht: Reidel), 127
Olson, E. C., & Etzel, P. B. 1993, AJ, 106, 342
Olson, E. C., & Etzel, P. B. 1995, AJ, 110, 2385
Shu, F. H. 1982, in The Physical Universe: An Introduction to Astronomy (Mill Valley, CA: Univ. Sci. Books), 90
Ulrich, R. K., & Burger, H. L. 1976, ApJ, 206, 509
Van Hamme, W. 1993, AJ, 106, 2096
Wilson, R. E. 1992, Documentation of Eclipsing Binary Computer Model (Gainesville, FL: Depart. Astron., Univ. Florida)